Design proposal:

Mach-Zehnder Interferometer

Natalia Balbastre Benavent

Natalia.balbastre@ipronics.com

Abstract: This report focuses on the design of a Mach-Zehnder interferometer implemented on a silicon-on-insulator platform using strip waveguide geometry. The work includes both numerical simulations and theoretical analysis to validate the proposed design.

Content

1. Introduction

Over the years, silicon photonics has become a key technology to address bandwidth demand and energy efficiency in optical communication systems. Its compatibility with standard CMOS manufacturing processes allows for the large-scale integration of high-performance optical components.

Regarding platforms for integrated photonics, SOI has emerged as one of the most widely adopted materials due to its compatibility with established CMOS fabrication processes, its ability to handle high-speed data, and the high index contrast that allows for compact, low-loss waveguides [1] [2]. The SOI structure is composed of a thin silicon layer, a buried oxide (BOX) layer, and a thick silicon substrate, which allows for efficient confinement of optical modes. While SOI is most effective for passive photonic devices, its disadvantage is that it does not support active components such as optical amplifiers or light sources [2].

The Mach-Zehnder Interferometer (MZI) is one of the key building blocks of integrated photonics, particularly in the development of optical modulators, switches, and filters. MZIs rely on the interference of light beams that traverse different optical paths to create a phase shift, which can be measured as a change in output intensity [3]. Due to their versatility, MZIs are integral to many applications in telecommunications, optical switching, and quantum computing, where precise control of light is essential. The ability to integrate MZIs on a silicon chip makes them highly attractive for large-scale, low-cost manufacturing, a major advantage in industries such as telecommunications, where minimizing size and cost while maintaining performance is critical [3].

On the other hand, MZIs introduce reconfigurability and flexibility into photonic devices. Programmable photonics refers to the ability to dynamically control the performance and functionality of optical circuits, such as switching between different transmission paths or adjusting signal modulation in real time. This flexibility is valuable in applications such as optical networks, where reconfigurable devices can adapt to changes in traffic patterns without requiring complete reconfiguration of the underlying physical infrastructure [4].

This report is centered on the design and simulation of MZI-based devices using the Silicon-on-Insulator (SOI) platform with strip waveguides. The strip waveguide design, typically fabricated in 220 nm silicon layers, allows for a compact structure with low propagation losses and high efficiency in terms of thermo-optic and electro-optic effects. These types of waveguides are well-suited for high-speed operation and can be integrated with other photonic components to form complex systems on a single chip.

The report is structured as follows:

- **Section 2:** Describes the principles of interferometry, the operational characteristics of the Mach-Zehnder Interferometer and its transfer function.

- **Section 3:** Discusses the design process for MZI-based devices, presents simulation results obtained in software application, and evaluates their performance under several conditions.

2. Theory of Mach-Zehnder Interferometer

The Mach-Zehnder Interferometer (MZI) operates by splitting an incoming optical signal into two output paths, introducing a phase difference, and then recombining them to observe interference effects. The theoretical model can be described as follows:
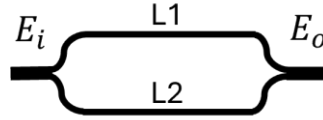
Initially, the input optical intensity I_i is equally divided by the first beam splitter:

$$I_1 = I_2 = \frac{Ii}{2}$$

Similarly, the electric fields in each arm are given by:

$$E_1 = E_2 = \frac{E_i}{\sqrt{2}}$$

At the second beam splitter, each field is again split into two components, resulting in:

$$E_{o1} = \frac{E_1}{\sqrt{2}} \qquad E_{o2} = \frac{E_2}{\sqrt{2}}$$

The propagation constant β is defined as:

$$\beta = \frac{2\pi n}{\lambda}$$

where n is the refractive index. During propagation, each field acquires a phase shift proportional to its path length L_1 and L_2.

$$E = E_0 e^{i(\omega t - \beta z)}$$

$$E_{o1} = E_1 e^{-i\beta L_1} = \frac{E_1}{\sqrt{2}} e^{-i\beta L_1}$$

$$E_{o2} = E_2 e^{-i\beta L_2} = \frac{E_2}{\sqrt{2}} e^{-i\beta L_2}$$

The output field E_o after recombination at the second beam splitter is the coherent sum of the two fields:

$$E_o = \frac{E_{o1} + E_{o2}}{\sqrt{2}} = \frac{E_i}{2} \left(e^{-i\beta L_1} + e^{-i\beta L_2} \right)$$

The output intensity I_o is then proportional to the square of the amplitude of E_o:

$$I_o = \frac{I_i}{4} \left| e^{-i\beta L_1} + e^{-i\beta L_2} \right|^2$$

Expanding this expression and using trigonometric identities, we obtain:

$$I_o = \frac{I_i}{2} (1 + \cos(\beta \Delta L))$$

where ΔL is the optical path difference between the two arms.

2.1. Free Spectral range

The **Free Spectral Range (FSR)** defines the wavelength separation between two consecutive maximum (or minimum) in the interference pattern and is given by:

$$FSR\,(\lambda) = \frac{\lambda^2}{\Delta L * n_g\,(\lambda)}$$

where $n_g\,(\lambda)$ is the group index of the waveguide defined as:

$$n_g\,(\lambda) = n_{eff}\,(\lambda) - \lambda \frac{dn_{eff}\,(\lambda)}{d\lambda}$$

Here, n_{eff} is the effective refractive index, which can vary with wavelength.

3. Modelling and simulation

3.1. Waveguide mode and analysis

The selected waveguide geometry is rectangular, with typical dimensions of 220 nm in height and 500 nm in width. A modal analysis was carried out using Lumerical MODE software to characterize the supported optical modes. The following simulation shows the mode profile (electric field intensity) of the fundamental quasi-TE mode, which exhibits a TE-like polarization with approximately 98% of the electric field aligned along the horizontal direction.
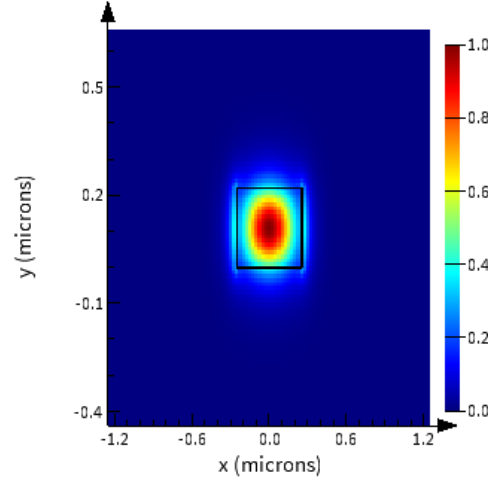
Figure 1. Mode profile (intensity E-field) of the first (quasi-) TE mode.

Then, a wavelength sweep was performed to evaluate both the effective index (n_{eff}) and the group index (n_g) across a range of wavelengths. This characterization is crucial for understanding the dispersion properties of the waveguide, which directly impact device performance in photonic circuits.

The variation of the effective index as a function of wavelength (λ) around 1550 nm can be accurately fitted using a second-order polynomial expression:

$$n_{eff}(\lambda) = n1 - n2 * (\lambda - 1.55) - n3 * (\lambda - 1.55)^2$$

where the fitted coefficients are n1= 2.446, n2=1.1534 and n3=0.0475.

Thus, the effective index as a function of wavelength is:

$$\boldsymbol{n_{eff}(\lambda) = 2.446 - 1.1534 * (\lambda - 1.55) - 0.0475 * (\lambda - 1.55)^2}$$
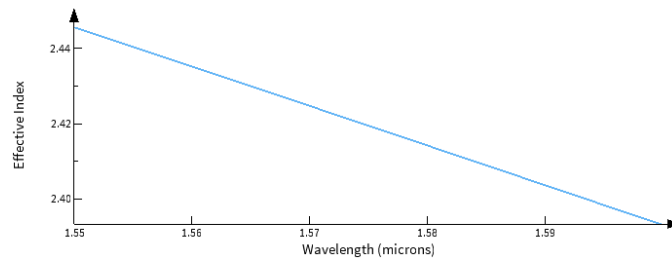
Figure 2. Effective index across wavelengths for TE1 mode.

On the other hand, the following figure represents the group index across wavelengths.
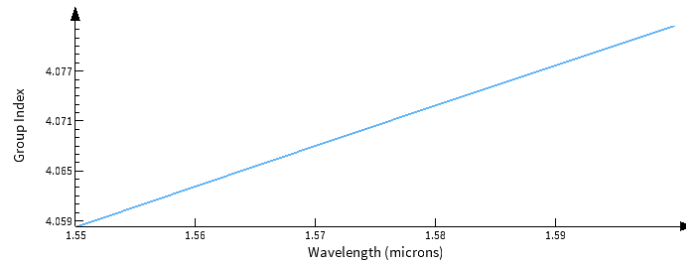
Figure 3. Group index across wavelengths for TE1 mode.

3.2. MZI modelling, simulation and analysis

Once the waveguide structure was defined, the optical circuit of the MZI was designed using Lumerical INTERCONNECT software which is a photonic integrated circuit simulation tool that enables the design and analysis of complex optical systems by modeling the behavior of interconnected optical components at the system level. It supports time-domain and frequency-domain simulations, allowing for performance evaluations of photonic devices.

MZI schematic is depicted in the following figure. The circuit consists of an Optical Network Analyzer (ONA), which characterizes the optical response of the circuit by measuring several parameters such as transmission, reflection, gain, losses and phase as functions of wavelength or frequency, a Y-branch splitter, two waveguides with different path lengths, and a Y-branch combiner.

The optical signal input is split by the Y-branch into two arms, propagates through waveguides of different lengths, and is subsequently recombined by the second Y-branch. The resulting interference pattern, determined by the optical path difference, is analyzed using the ONA to assess the MZI performance.
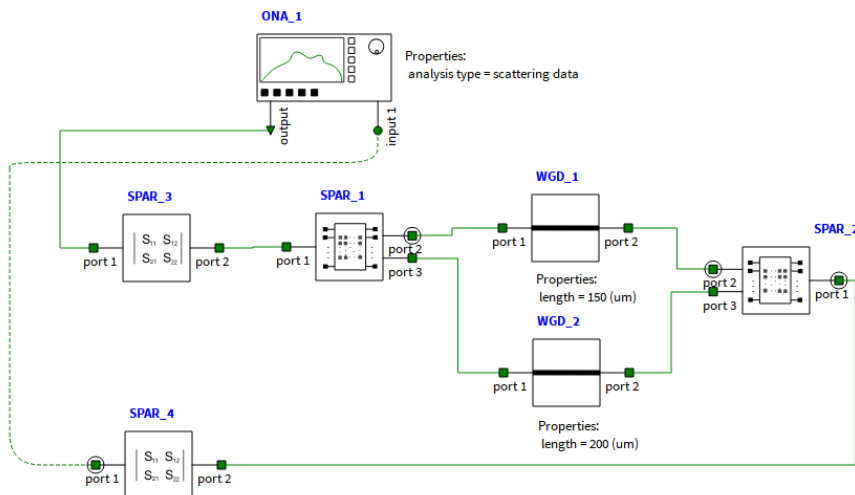

Figure 4. MZI schematic using Lumerical INTERCONNECT.

6

Once the circuit is designed, an individual characterization is performed. For this purpose, the grating coupler (GC) was connected to the Optical Network Analyzer (ONA), as shown in Figure 5. Following the simulation, the insertion loss as a function of wavelength was extracted and is illustrated in Figure 6.
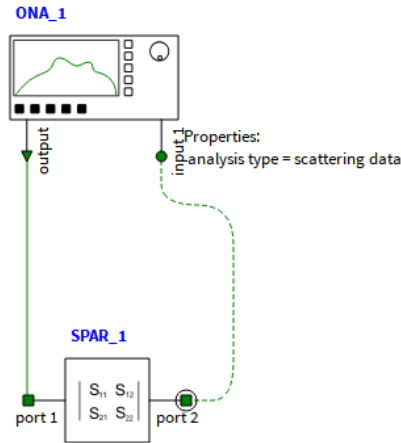

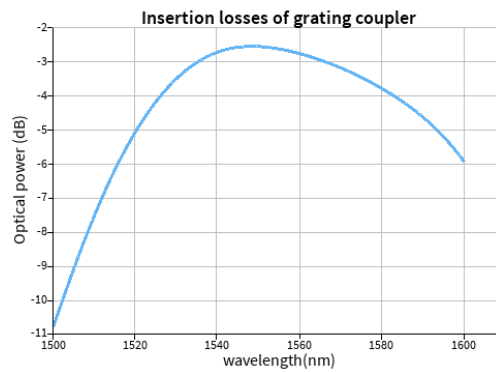*Figure 4. Grating Coupler schematic using Lumerical INTERCONNECT.*

Figure 5. Grating coupler transfer function.

Similarly, the Y-branch was characterized by connecting it to the ONA to evaluate its insertion losses across wavelengths.
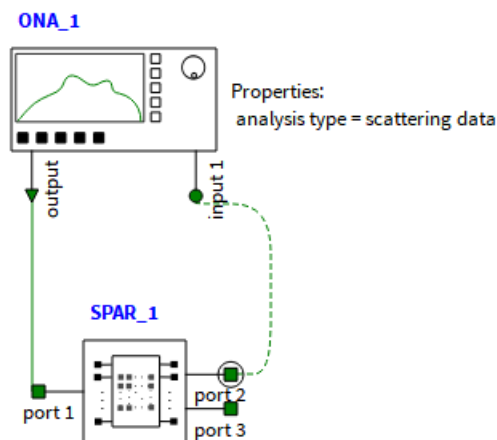
Figure 6. Y-Branch schematic using Lumerical INTERCONNECT.
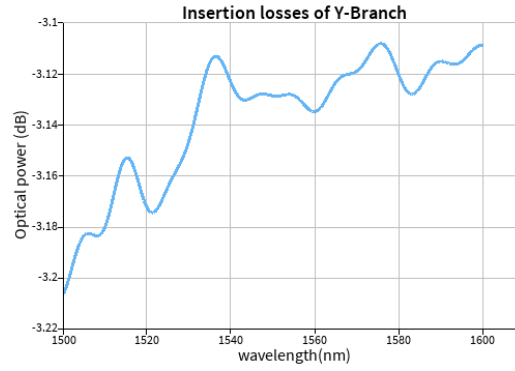
Figure 7. Y-Branch transfer function.

Once the Y-branch and GC were characterized, the transfer function of the MZIs was simulated for different path length mismatches (ΔL) between its two waveguides. The length of the upper waveguide was fixed at 150 µm, while the length of the lower waveguide was varied in steps of 50 µm, resulting in lengths of 200 µm, 250 µm, 300 µm, 350 µm and 400 µm. As shown in Figure 9, FSR decreases as the path length difference (ΔL) increases.
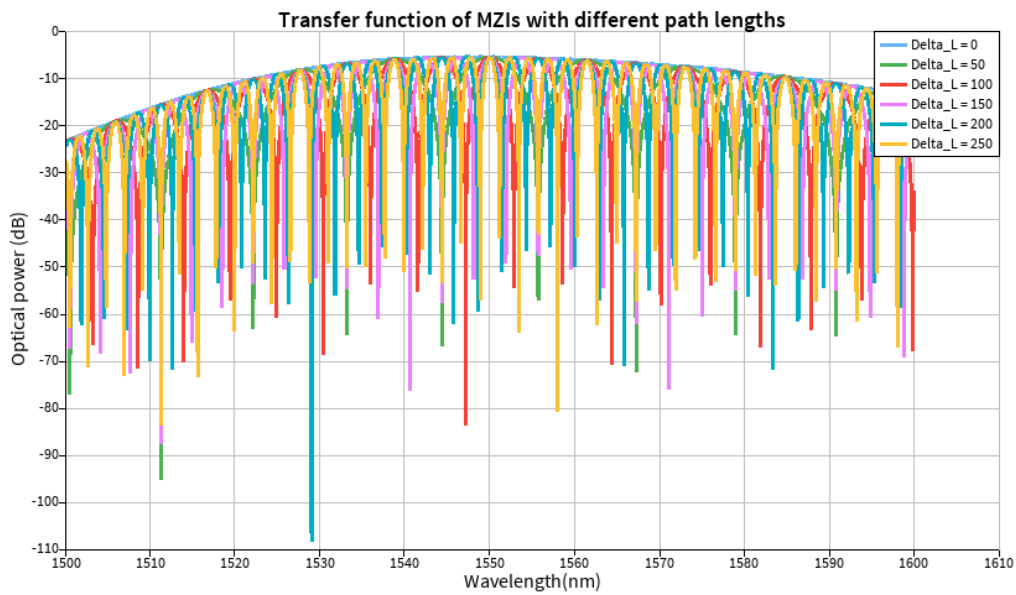

Figure 8. Transfer function of MZIs with different path lengths.

On the other hand, the transmission spectrum for TE polarization of each MZI is represented in Figure 10.
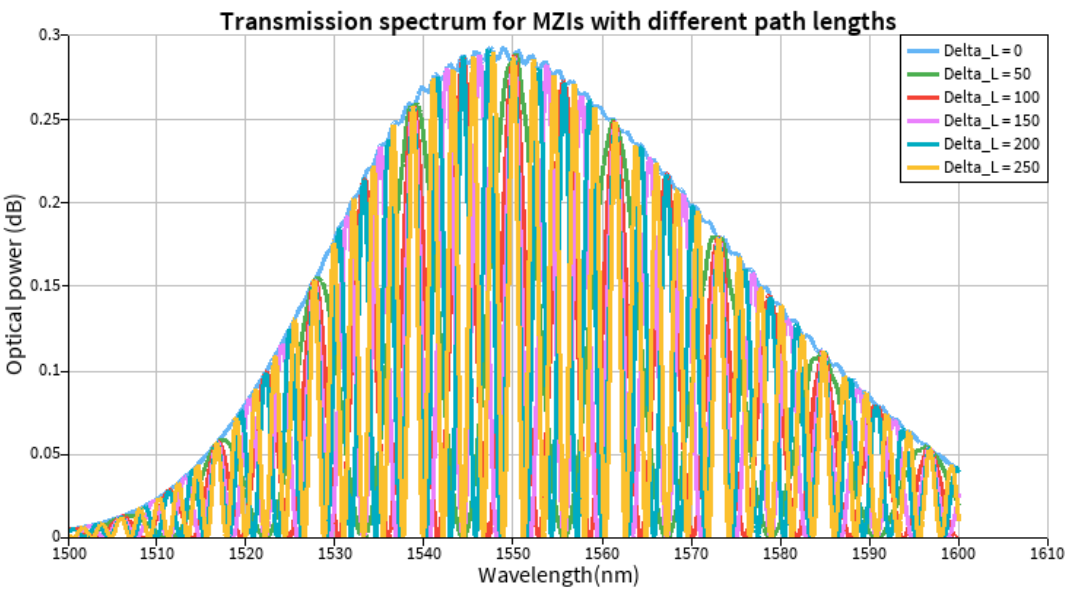
Figure 9. Transmission spectrum of MZIs with different path lengths.

Using the script prompt in Lumerical INTERCONNECT, the approximate value of the "Free Spectral Range" at "Result View – ONA_1" was obtained for each unbalanced MZI configuration in Figure 10. Then, Table 1 summarizes the FSR for each MZI.
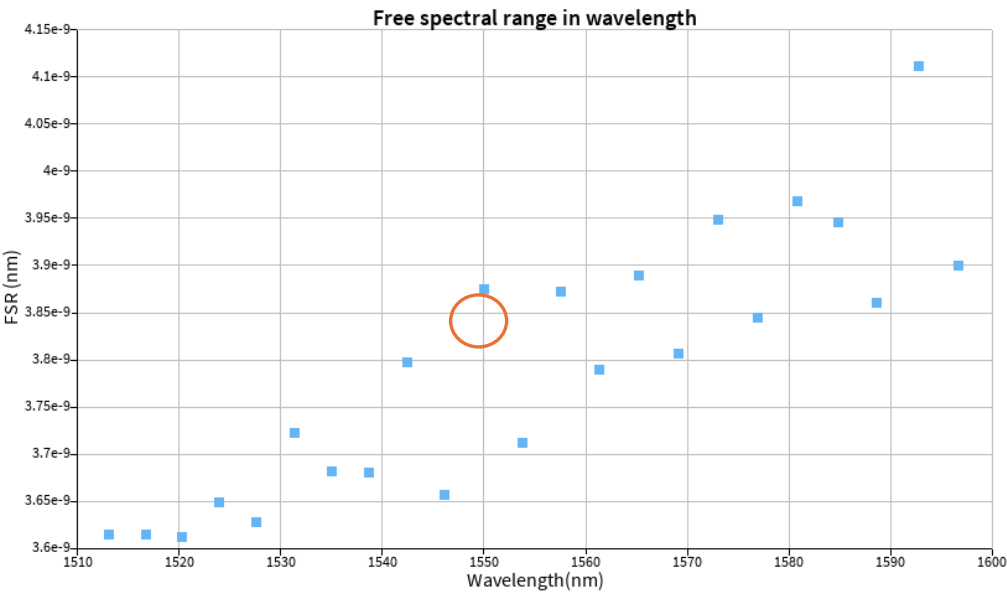

Figure 10. FSR for ΔL = 150 µm.

Simulated results for each MZI			
Components	Length path WG 1 (µm)	Length path WG 2 (µm)	FSR (nm) @1550 nm
MZI 1	150	200	11.05
MZI 2	150	250	5.74
MZI 3	150	300	3.87
MZI 4	150	350	2.84
MZI 5	150	400	2.32

Table 1. Simulated FSR for each MZI.

4. Additional structures

Once the FSR study was completed, new MZIs were designed and integrated into the circuit layout. These structures include several variations in optical path lengths, as well as a splitter, to enable a more detailed characterization of their spectral behavior.

In this section, the gain spectra of two of these new structures, MZI 6 and MZI 7, will be presented and analyzed. These identifiers correspond to the names assigned in the layout to clearly distinguish each interferometer.
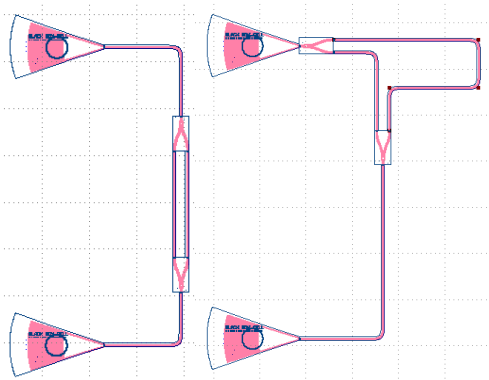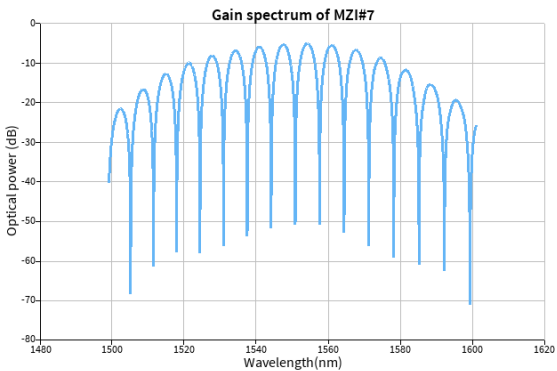

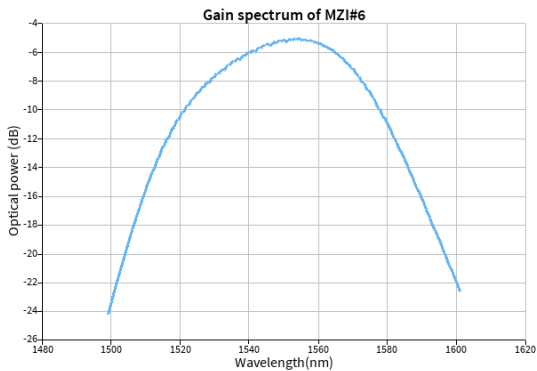*Figure 12. MZI6   Figure 13. MZI7*

Figure 14. Gain spectrum of MZI#7   Figure 15. Gain spectrum of MZI#6

10

On the other hand, a splitter has been included to evaluate its behavior. The schematic of the splitter is depicted in Figure 16.
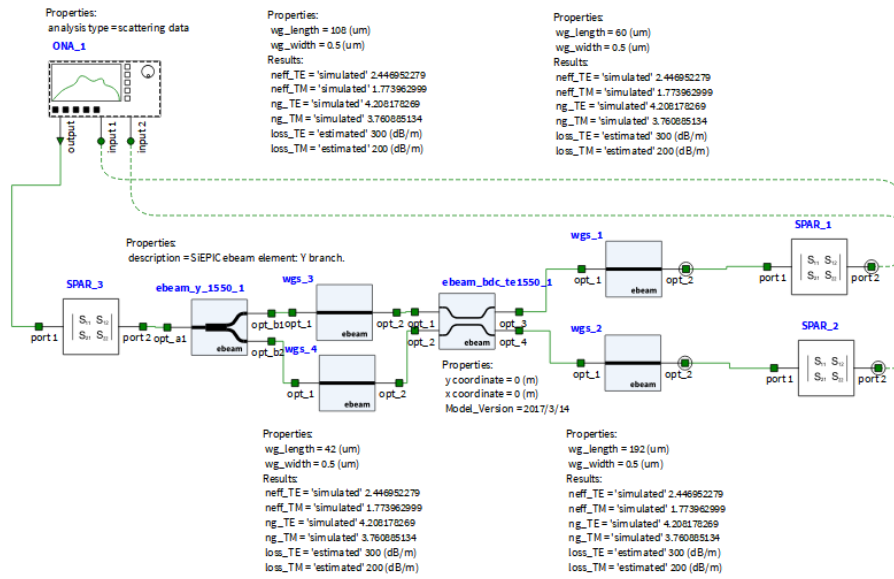

Figure 16. Splitter schematic using Lumerical INTERCONNECT.

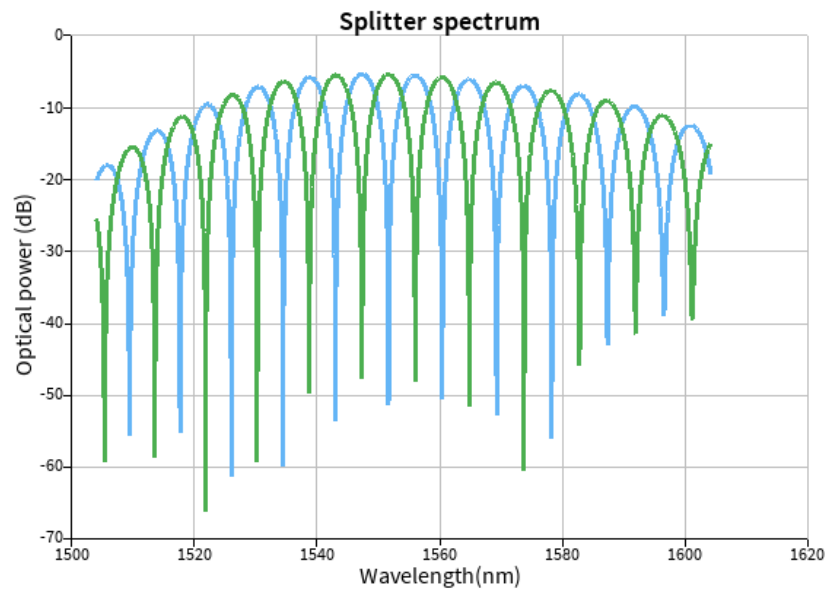The following figure represents the gain spectrum of each input.

Figure 17. Splitter's gain spectrum using Lumerical INTERCONNECT.

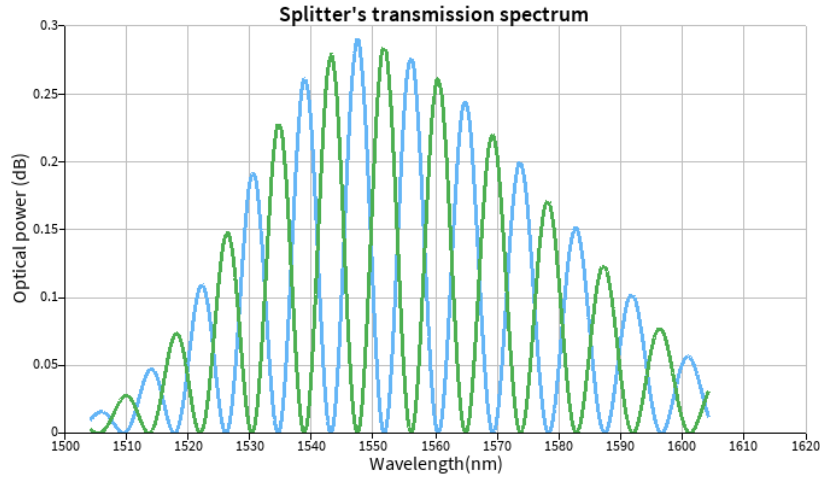Additionally, the splitter's transmission spectrum for each input is represented in the following figure:

Figure 18. Splitter's transmission spectrum using Lumerical INTERCONNECT.

5. Layout

This section describes the final design proposal, and the layout mask created in KLayout software. The design includes seven MZIs with different path lengths, one calibration loop, and one splitter for performance evaluation. All components are designed for TE polarization.

Several considerations were considered during the mask design to enable automated measurements. The chip dimensions were fixed at 605 x 410 µm. TE grating couplers are oriented to the right side with a pitch of 127 µm. Additionally, all waveguide bends were designed with a radius of 5 µm to minimize bend losses.
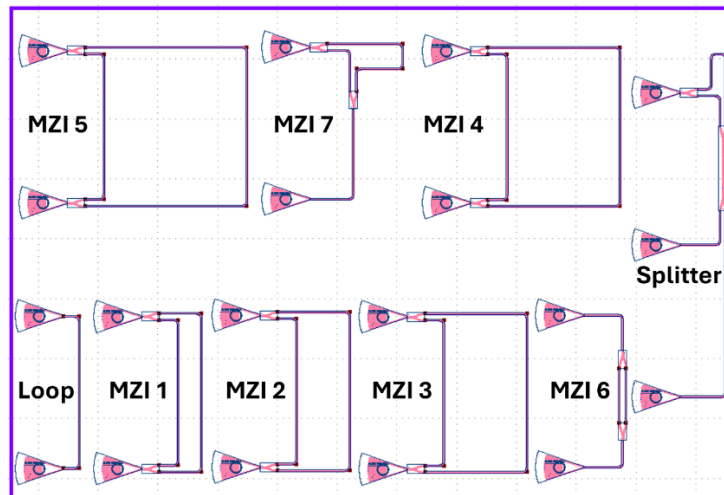

Figure 118. Final design mask created in KLayout.

Regarding MZIs 1 to 5, the only difference among them lies in the path length of the second waveguide. In addition to these, two alternative designs of MZIs (MZI 6 and MZI 7) were also included to evaluate other performance.

Components	Length path WG 1 (µm)	Length path WG 2 (µm)
Loop	150	-
MZI 1	150	200
MZI 2	150	250
MZI 3	150	300
MZI 4	150	350
MZI 5	150	400
MZI 6	53.5	60.5
MZI 7	50	136

Table 2. Design variations of each component.

6. Manufacturing variability

Once the chips are designed, they are sent for fabrication using electron beam lithography. In this process, the design pattern is transferred onto an electron beam resist, which serves to protect the waveguides during the etching process. After etching, the waveguides are encapsulated with an oxide layer.

This fabrication process is subject to variations in waveguide thickness and width, which can significantly affect key performance metrics such as the MZI transmission peak wavelength, device insertion loss, group index, FSR, extinction ratio, and others.

To predict these variations, a technique known as corner analysis is employed. This method helps to predict the impact of typical fabrication and environmental variations on device performance.

Assuming wafer thickness variations between 215.3 nm and 223.1 nm, and waveguide width variations between 470 nm and 510 nm, simulations were done using Lumerical MODE. The waveguide width and thickness were systematically varied to extract and evaluate the resulting changes in key parameters such as the group index, effective index and FSR.

The following table summarizes these parameters for TE polarization at 1550 nm:

TE polarization @ 1550 nm					
Variation	Thickness (nm)	Width (nm)	Vg	ng	neff	FSR (nm)
1	215.3	470	7.09044e7	4.22812	2.3698	5.6822
2	215.3	510	7.21008e7	4.15796	2.4375	5.7780
3	220	500	7.17732e7	4.17694	2.4404	5.7518
4	223.1	470	7.07595e7	4.23678	2.3985	5.6706
5	223.1	510	7.19762e7	4.16561	2.4659	5.7681

Table 3. FSR, ng and neff evaluation varying thickness and width.

Once the key parameters are obtained, the compact models for the corner analysis are defined:

	TE polarization @ 1550 nm		
Variation	Thickness (nm)	Width (nm)	Waveguides compact model
1	215.3	470	$n_{eff}(\lambda) = 2.36982 - 1.1962 * (\lambda - 1.55) - 0.0412 * (\lambda - 1.55)^2$
2	215.3	510	$n_{eff}(\lambda) = 2.4375 - 1.1064 * (\lambda - 1.55) - 0.0461 * (\lambda - 1.55)^2$
3	220	500	$n_{eff}(\lambda) = 2.446 - 1.1534 * (\lambda - 1.55) - 0.0475 * (\lambda - 1.55)^2$
4	223.1	470	$n_{eff}(\lambda) = 2.3985 - 1.185 * (\lambda - 1.55) - 0.0433 * (\lambda - 1.55)^2$
5	223.1	510	$n_{eff}(\lambda) = 2.4659 - 1.0966 * (\lambda - 1.55) - 0.0466 * (\lambda - 1.55)^2$

Table 4. Waveguide compact model for the corner analysis

All data extracted for the corner analysis across the full wavelength range are shown below. The following figure displays the dependence of the effective index and group index on wavelength for each compact model. As the waveguide width increases, from 470 nm to 510 nm, both n_{eff} and n_g increase, due to stronger mode confinement. Similarly, increasing the waveguide thickness, from 215.3 nm to 223.1 nm, also shows higher indices.

On the other hand, the effective index decreases with wavelength, which indicates normal dispersion behavior. Meanwhile, the group index shows a slight increase with wavelength.
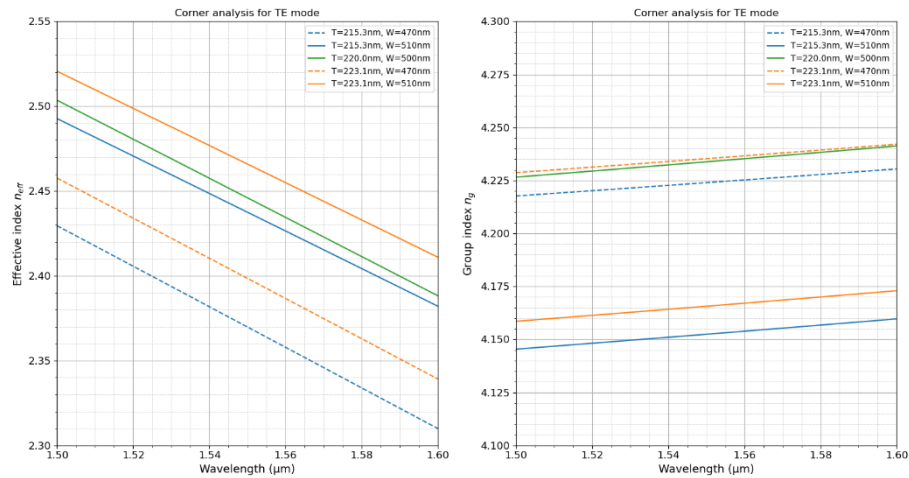

Figure 12. Effective index and group index for corner analysis.

To sum up, the effective index ranges approximately from 2.37 to 2.466, while the group index varies between 4.158 and 4.237.

Moreover, Monte Carlo simulations carried out in KLayout allow for the prediction of variations in peak wavelength, peak gain, and FSR. These simulations are performed on 10 dies per wafer to evaluate inter-wafer manufacturing variability. To analyze this variability, histograms have been generated for each designed component, as illustrated below:
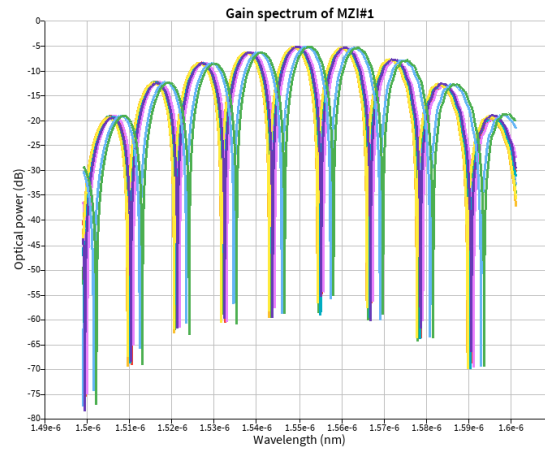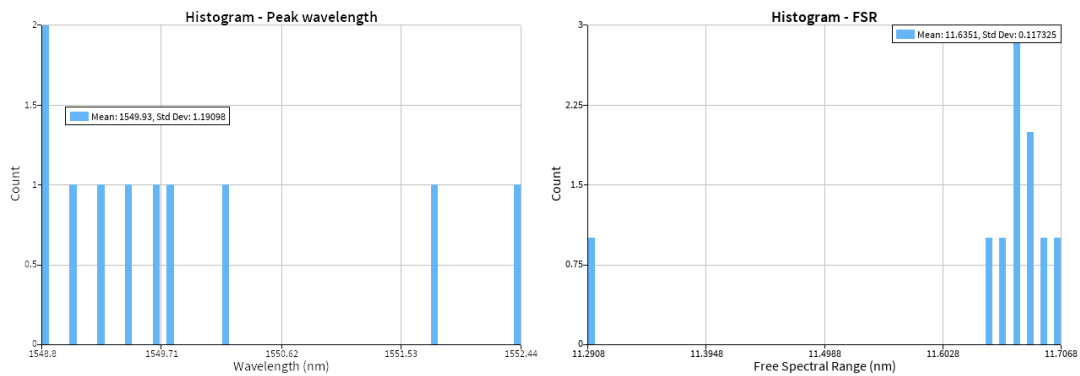

Figure 13. MZI#1 gain spectrum of 10 dies using Monte Carlo simulations.

Analyzing the gain spectrum, a shift can be observed in each simulation. On the other hand, many histograms have been obtained to evaluate the mean peak of wavelength, the mean peak of gain and the FSR of 10 dies and its corresponding standard deviation.
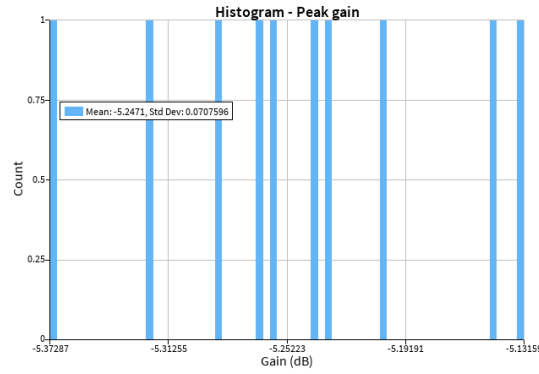
Figure 14. FSR, peak gain and peak wavelength for 10 dies.

Similar graphs have been obtained for the remaining components, and the key parameters are summarized in the table below:

Monte Carlo simulations						
Component	Mean FSR	Std FSR	Mean Peak Gain (dB)	Std Peak Gain (dB)	Mean Peak Wvl (nm)	Std Peak Wvl (nm)
Loop	-	-	-5.87	0.18	1559.58	0.918
MZI 1	11.63	0.117	-5.24	0.07	1549.93	1.191
MZI 2	5.69	0.035	-5.32	0.07	1548.43	0.827
MZI 3	3.77	0.009	-6.04	0.16	1547.86	0.374
MZI 4	2.89	0.016	-6.71	0.21	1548.34	0.708
MZI 5	2.28	0.012	-5.44	0.05	1548.54	0.693
MZI 6	-	-	-5.47	0.28	1559.99	1.721
MZI 7	6.73	0.09	-5.64	0.43	1548.47	2.5

Table 5. Monte Carlo simulations for each MZI.

7. Experimental data

To characterize the devices, a custom-built automated test setup [5] [6] with automated control software written in Python was used [7]. An Agilent 81600B tunable laser was used as the input source and Agilent 81635A optical power sensors as the output detectors. The wavelength was swept from 1500 to 1600 nm in 10 pm steps. A polarization maintaining (PM) fibre was used to maintain the polarization state of the light, to couple the TE polarization into the grating couplers [8]. A 90º rotation was used to inject light into the TM grating couplers [8]. A polarization maintaining fibre array was used to couple light in/out of the chip [9].

The experimental data will be analyzed for all the designed structures; however, to limit the scope of the analysis, detailed data and graphs will be presented for a

specific MZI under TE polarization (**MZI 2**) which has an FSR of 5.7 nm and a path length difference of 100 μm.

On the one hand, a loop-back structure composed of two grating couplers connected by a waveguide was introduced. This configuration is used to eliminate the effect of the grating couplers from the experimental MZI transmission spectrum.
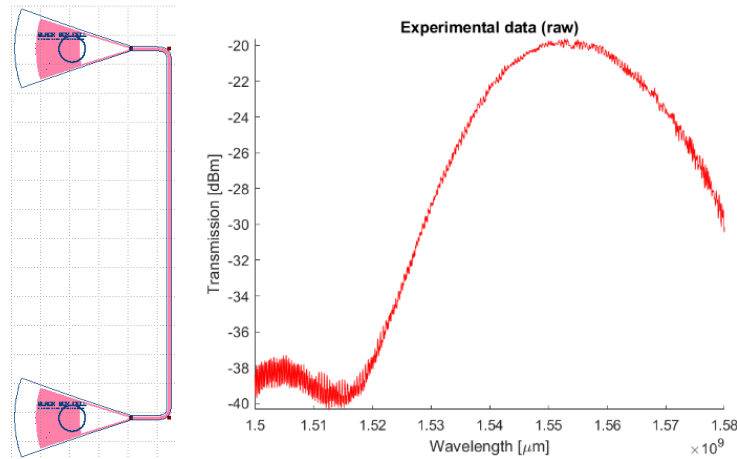

Figure 15. Design and transmission spectrum loop.

In the following figure, a baseline correction is applied. This method consists of a polynomial fit that estimates the gratings transfer function. In this case, the polynomial order applied is 4.
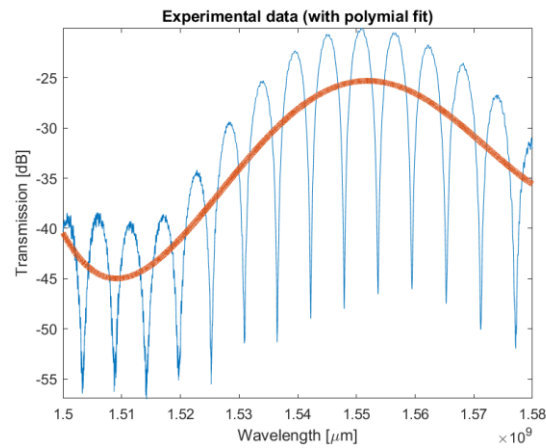
Figure 16. Transmission spectrum with polynomial fit of MZI2.

As an example of fitting an MZI using the autocorrelation method, all the steps followed are summarized in the figure below, using MZI 2 as a case study. Note that it is represented from 1520 nm to 1570 nm because the first 20 nm are limited by the noise floor. First, Figure (a) shows the experimental data after baseline correction. Then, the autocorrelation is applied in Figure (b), and the experimental data is shifted to misalign the spectrum with the initial one in Figure (c). Finally, using this shift, a perfect match between both spectra is achieved in Figure (d), allowing the extraction of the group index from the fitting in Figure (f).
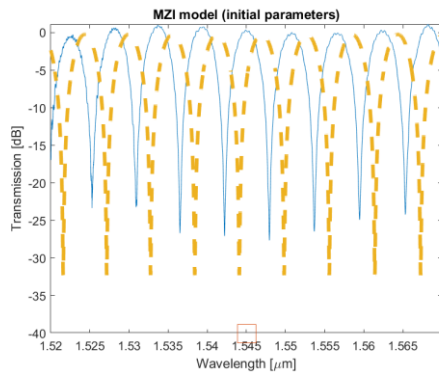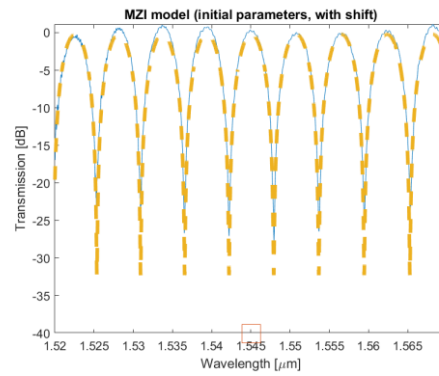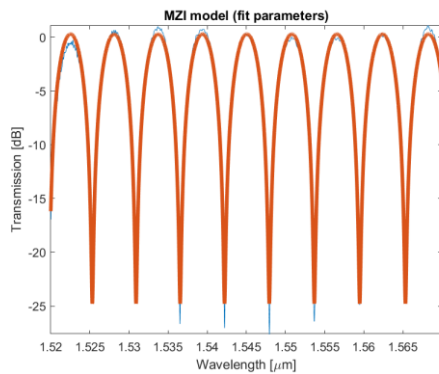
a) Experimental data (baseline corrected, wavelength range)

b) Autocorrelation of spectrum

c) MZI model (initial parameters)

d) MZI model (initial parameters, with shift)

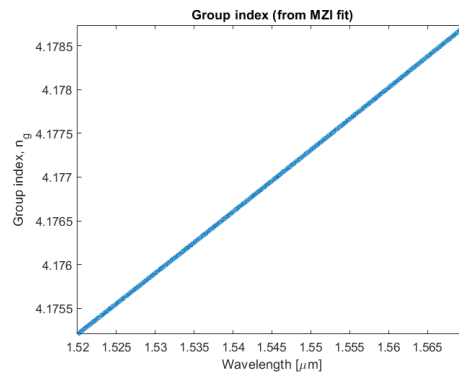**e)** MZI model (fit parameters)

f) Group index (from MZI fit)
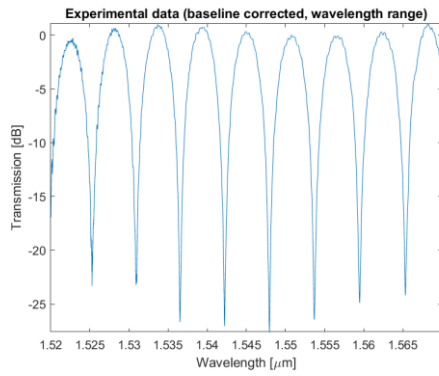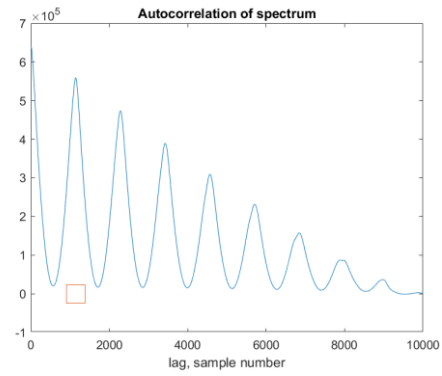
In the same way, the correlation fitting method was applied to the rest of the MZIs.

In the following figures, it is summarized the comparison between nominal simulations and the experimental data. Note that MZI 6 does not appear because its path length difference is not enough to have a FSR as can be seen in the figure below:
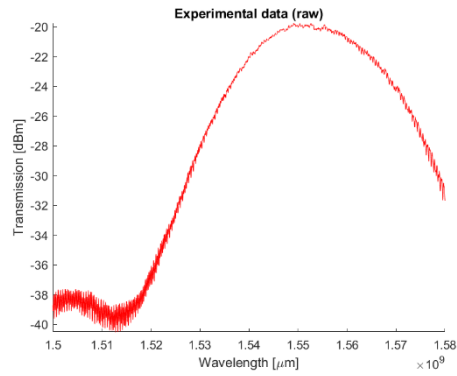
Figure 17. Transmission spectrum of MZI6.
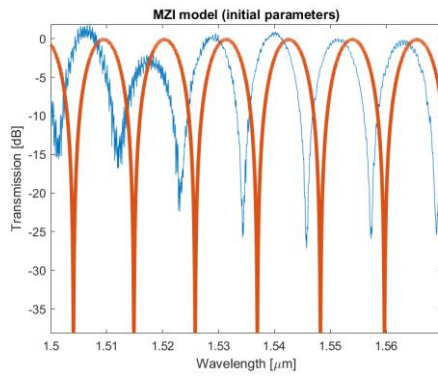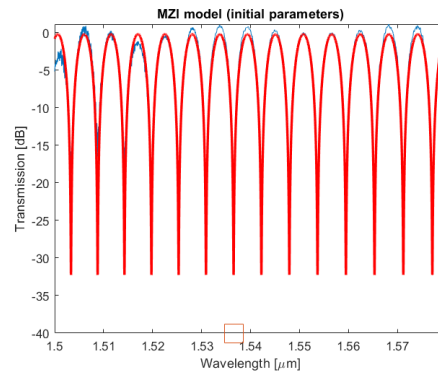

Figure 18. Transmission spectrum of MZI1.   *Figure 19. Transmission spectrum of MZI2.*
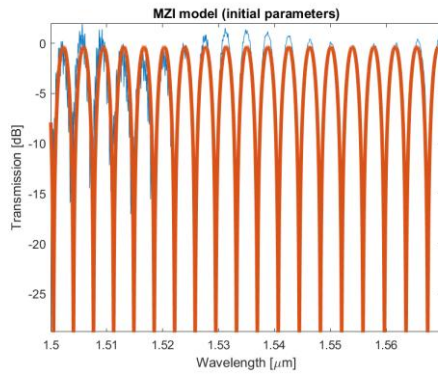

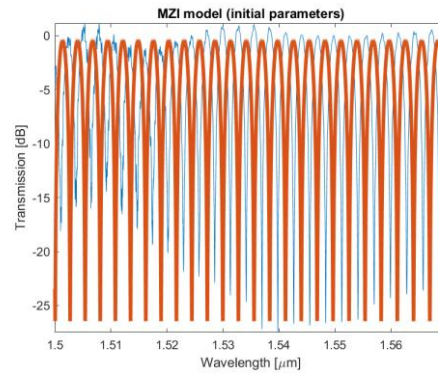*Figure 20. Transmission spectrum of MZI3.*   *Figure 21. Transmission spectrum of MZI4.*
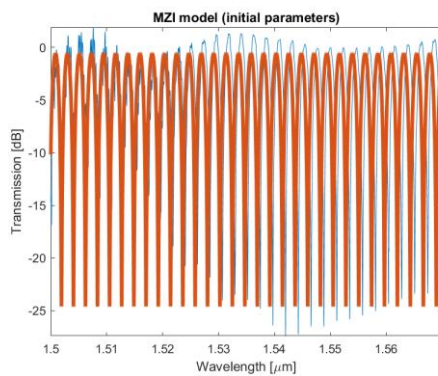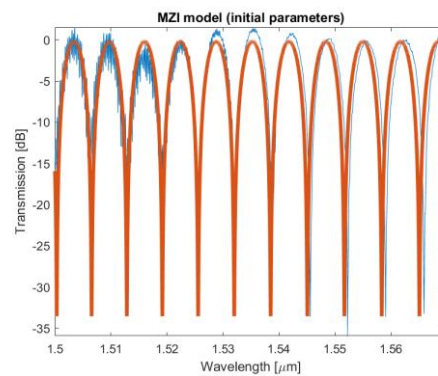

Figure 22. Transmission spectrum of MZI5.   *Figure 23. Transmission spectrum of MZI7.*

As observed in Figure 18, there is a mismatch between the nominal simulation and the experimental data. To address this, a fitted simulation is performed to achieve a perfect match between both spectra. However, for the remaining MZIs, this step is not necessary, as the initial parameters already result in an excellent match:
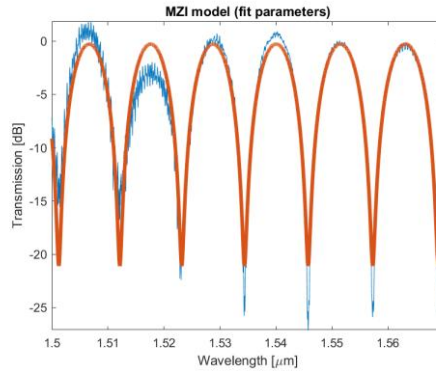

Figure 24. Transmission spectrum fitted of MZI1.

Finally, the key parameters simulated and measured are summarized in Table 6. As can be seen, the FSR values match very well between simulation and measurement, and the ng values fall within the range considered in the corner analysis.

Summary of simulation and experimental results					
Component	ΔL (µm)	FSR simulated	FSR experimental	ng simulated	Ng experimental
MZI 1	50	11.63	11.50	4.132	4.171
MZI 2	100	5.69	5.69	4.222	4.181
MZI 3	150	3.79	3.80	4.226	4.180
MZI 4	200	2.89	2.86	4.156	4.178
MZI 5	250	2.28	2.29	4.215	4.181
MZI 7	86	6.73	6.70	4.188	4.143

Table 6. Summary of simulation and experimental results.

Acknowledgments

References

[1] D. Thomson, «Roadmap on silicon photonics,» *Journal of Optics,* nº 7, p. 21, 2016.

[2] L. V. a. L. P. (Eds.), Handbook of Silicon Photonics, CRC Press, 2013.

[3] J. Y. a. J. C. D. Marpaung, «Integrated microwave photonics,» *Nature Photonics,* vol. 12, p. 90, 2019.

[4] I. G. a. J. C. D. Pérez, «Programmable multifunctional photonics ICs,» *IEEE Journal of Selected Topics in Quantum Electronics,* p. 11, 2018.

[5] R. J. Bojko, J. Li, L. He, T. Baehr-Jones, M. Hochberg, and Y. Aida, "Electron beam lithography writing strategies for low loss, high confinement silicon optical waveguides," J. Vacuum Sci. Technol. B 29, 06F309 (2011)

[6] Lukas Chrostowski, Michael Hochberg, chapter 12 in "Silicon Photonics Design: From Devices to Systems", Cambridge University Press, 2015

[7] http://siepic.ubc.ca/probestation, using Python code developed by Michael Caverley.

[8] Yun Wang, Xu Wang, Jonas Flueckiger, Han Yun, Wei Shi, Richard Bojko, Nicolas A. F. Jaeger, Lukas Chrostowski, "Focusing sub-wavelength grating couplers with low back reflections for rapid prototyping of silicon photonic circuits", Optics Express Vol. 22, Issue 17, pp. 20652-20662 (2014) doi: 10.1364/OE.22.020652

[9] www.plcconnections.com, PLC Connections, Columbus OH, USA.